

Comparative analysis of the $\Lambda_b \rightarrow \Lambda \ell^+ \ell^-$ decay in the SM, SUSY, and RS model with custodial protection

K. Azizi,^{1,*} A. T. Olgun,^{2,†} and Z. Tavukoğlu^{2,‡}¹*Department of Physics, Doğuş University, Acıbadem-Kadıköy, 34722 İstanbul, Turkey*²*Vocational School Kadıköy Campus, Okan University, Hasanpaşa-Kadıköy, 34722 İstanbul, Turkey*
(Received 2 October 2015; published 30 December 2015)

We comparatively analyze the rare $\Lambda_b \rightarrow \Lambda \ell^+ \ell^-$ channel in the standard model, supersymmetry, and Randall-Sundrum model with custodial protection (RS_c). Using the parametrization of the matrix elements entering the low-energy effective Hamiltonian in terms of form factors, we calculate the corresponding differential decay width and lepton forward-backward asymmetry in these models. We compare the results obtained with the most recent data from LHCb as well as lattice QCD results on the considered quantities. It is obtained that the standard model, with the form factors calculated in light-cone QCD sum rules, cannot reproduce some experimental data on the physical quantities under consideration, but the supersymmetry model can do it. The RS_c model predictions are roughly the same as the standard model, and there are no considerable differences between the predictions of these two models. In the case of differential decay rate, the data in the range $4 \text{ GeV}^2/c^4 \leq q^2 \leq 6 \text{ GeV}^2/c^4$ cannot be described by any of the considered models.

DOI: [10.1103/PhysRevD.92.115025](https://doi.org/10.1103/PhysRevD.92.115025)

PACS numbers: 12.60.-i, 12.60.Jv, 13.30.-a, 13.30.Ce

I. INTRODUCTION

The ATLAS and CMS Collaborations at CERN have independently reported their discovery of the Higgs boson with a mass of about 125 GeV using the samples of proton-proton collision data collected in 2011 and 2012, commonly referred to as the first LHC run [1–3]. Recently, a measurement of the Higgs boson mass based on the combined data samples of the ATLAS and CMS experiments has been presented as $m_H = 125.09 \pm 0.21(\text{stat}) \pm 0.11(\text{syst})$ GeV in Refs. [3–7]. At the same time, all LHC research for signals of new physics above the TeV scale have given negative results. However, the LHC constraints on new physics effects can help theoreticians in the course of searching for these new effects and answering the questions that the standard model (SM) has not answered yet. We hope that the upcoming LHC run can bring unexpected opportunities to observe signals of new physics in the experiment [8].

Although the SM could be valid up to some arbitrary high scale, new scenarios should exist because we are lacking a proper understanding of some important issues like the origin of the matter, matter-antimatter asymmetry, dark matter and dark energy, etc. [9]. In the baryonic sector, the loop-induced flavor-changing neutral current (FCNC) decay of the $\Lambda_b \rightarrow \Lambda \ell^+ \ell^-$ with $\ell = e, \mu, \tau$, which is described by the $b \rightarrow s \ell^+ \ell^-$ transition at quark level, is one of the important rare processes that can help us in the course of indirectly searching for new physics effects [10]. Recently, the differential branching fraction of the

$\Lambda_b^0 \rightarrow \Lambda \mu^+ \mu^-$ decay channel has been measured as a function of the square of the dimuon invariant mass (q^2), corresponding to an integrated luminosity of 3.0 fb^{-1} using proton-proton collision data collected by the LHCb experiment [11]. The measured result at the $15 \text{ GeV}^2/c^4 \leq q^2 \leq 20 \text{ GeV}^2/c^4$ region for the differential branching fraction is $d\text{Br}(\Lambda_b^0 \rightarrow \Lambda \mu^+ \mu^-)/dq^2 = (1.18_{-0.08}^{+0.09} \pm 0.03 \pm 0.27) \times 10^{-7} \text{ GeV}^2/c^4$. The LHCb Collaboration has also reported the measurement on the forward-backward asymmetries of this transition at the μ channel. The measured result at the $15 \text{ GeV}^2/c^4 \leq q^2 \leq 20 \text{ GeV}^2/c^4$ region for the lepton forward-backward asymmetry is $A_{\text{FB}}^\mu = -0.05 \pm 0.09(\text{stat}) \pm 0.03(\text{syst})$ [11]. In the literature, there are a lot of studies on this decay channel via different approaches (for some recent studies, see for instance Refs. [12–17]).

In the present work, we calculate the differential decay rate and lepton forward-backward asymmetry related to the FCNC $\Lambda_b \rightarrow \Lambda \ell^+ \ell^-$ transition for all leptons in the SM, supersymmetry (SUSY), and Randall-Sundrum scenarios with custodial protection (RS_c). We compare the results with the experimental data provided by LHCb [11] as well as the existing lattice QCD predictions [18]. Comparison of the LHCb results with the lattice QCD predictions shows that there are some deviations of data from the SM predictions. Such deviations can be attributed to the new physics effects that can contribute to such loop-level processes. In this connection, we comparatively analyze the $\Lambda_b \rightarrow \Lambda \ell^+ \ell^-$ decay channel in SM and some new physics scenarios. In the calculations, we use the form factors calculated via the light-cone QCD sum rules in Ref. [19]. Hence, to avoid misleading, we will use SMLCSR instead of SM to refer to the results that are

*kazizi@dogus.edu.tr

†tugba.olgun@okan.edu.tr

‡zeynep.tavukoglu@okan.edu.tr

obtained using the form factors predicted by the light-cone sum rules in Ref. [19] when we speak about the predictions of different models. Note that there are many studies devoted to the calculation of the form factors defining the transition under consideration via different approaches (see for instance Refs. [17,20]), but our aim here is to use those form factors that are obtained in the full theory of QCD in Ref. [19] without any approximation.

The outline of the paper is as follows: In the next section, we introduce a detailed discussion of the effective Hamiltonian responsible for the semileptonic $\Lambda_b \rightarrow \Lambda \ell^+ \ell^-$ decay channel and Wilson coefficients in SM, RS_c , and SUSY models. In this section, we also present a basic introduction of the RS_c scenario. In Sec. III, we calculate the differential decay rate and lepton forward-backward asymmetry at different scenarios and compare the predictions of different models.

II. THE SEMILEPTONIC $\Lambda_b \rightarrow \Lambda \ell^+ \ell^-$ TRANSITION IN SM, SUSY, AND RS_c MODELS

A. The effective Hamiltonian and Wilson coefficients

At quark level, the FCNC transition of $\Lambda_b \rightarrow \Lambda \ell^+ \ell^-$ is governed by the $b \rightarrow s \ell^+ \ell^-$ transition, whose effective Hamiltonian in the SM can be written as

$$\begin{aligned} \mathcal{H}_{\text{SM}}^{\text{eff}} = & \frac{G_F \alpha_{em} V_{tb} V_{ts}^*}{2\sqrt{2}\pi} [C_9^{\text{eff,SM}} \bar{s} \gamma_\mu (1 - \gamma_5) b \bar{\ell} \gamma^\mu \ell \\ & + C_{10}^{\text{SM}} \bar{s} \gamma_\mu (1 - \gamma_5) b \bar{\ell} \gamma^\mu \gamma_5 \ell \\ & - 2m_b C_7^{\text{eff,SM}} \frac{1}{q^2} \bar{s} i \sigma_{\mu\nu} q^\nu (1 + \gamma_5) b \bar{\ell} \gamma^\mu \ell], \end{aligned} \quad (2.1)$$

where V_{tb} and V_{ts}^* are elements of the Cabibbo-Kobayashi-Maskawa (CKM) mixing matrix; α_{em} is the fine structure constant at Z mass scale; G_F is the Fermi weak coupling constant; q^2 is the transferred momentum squared; and $C_9^{\text{eff,SM}}$, C_{10}^{SM} , and $C_7^{\text{eff,SM}}$ are the Wilson coefficients representing different interactions. The explicit expressions of the Wilson coefficients entered into the above Hamiltonian are given in the following equations. The Wilson coefficient $C_9^{\text{eff,SM}}$, which is a function of $\hat{s}' = \frac{q^2}{m_b^2}$ where q^2 lies in the allowed region $4m_l^2 \leq q^2 \leq (m_{\Lambda_b} - m_\Lambda)^2$, is given by [21,22]

$$\begin{aligned} C_9^{\text{eff,SM}}(\hat{s}') = & C_9^{\text{NDR}} \eta(\hat{s}') + h(z, \hat{s}') \\ & \times (3C_1 + C_2 + 3C_3 + C_4 + 3C_5 + C_6) \\ & - \frac{1}{2} h(1, \hat{s}') (4C_3 + 4C_4 + 3C_5 + C_6) \\ & - \frac{1}{2} h(0, \hat{s}') (C_3 + 3C_4) \\ & + \frac{2}{9} (3C_3 + C_4 + 3C_5 + C_6), \end{aligned} \quad (2.2)$$

where C_9^{NDR} in the naive dimensional regularization (NDR) scheme is expressed as

$$C_9^{\text{NDR}} = P_0^{\text{NDR}} + \frac{Y^{\text{SM}}}{\sin^2 \theta_W} - 4Z^{\text{SM}} + P_E E^{\text{SM}}. \quad (2.3)$$

The last term on the right-hand side is neglected due to the smallness of the order of P_E . Here $P_0^{\text{NDR}} = 2.60 \pm 0.25$, $Y^{\text{SM}} = 0.98$, $Z^{\text{SM}} = 0.679$, and $\sin^2 \theta_W = 0.23$ [21–23]. The parameter $\eta(\hat{s}')$ in Eq. (2.2) is given as

$$\eta(\hat{s}') = 1 + \frac{\alpha_s(\mu_b)}{\pi} \omega(\hat{s}'), \quad (2.4)$$

with

$$\begin{aligned} \omega(\hat{s}') = & -\frac{2}{9} \pi^2 - \frac{4}{3} \text{Li}_2(\hat{s}') - \frac{2}{3} \ln \hat{s}' \ln(1 - \hat{s}') \\ & - \frac{5 + 4\hat{s}'}{3(1 + 2\hat{s}')} \ln(1 - \hat{s}') - \frac{2\hat{s}'(1 + \hat{s}')(1 - 2\hat{s}')}{3(1 - \hat{s}')^2(1 + 2\hat{s}')} \ln \hat{s}' \\ & + \frac{5 + 9\hat{s}' - 6\hat{s}'^2}{6(1 - \hat{s}')(1 + 2\hat{s}')} \end{aligned} \quad (2.5)$$

and

$$\alpha_s(x) = \frac{\alpha_s(m_Z)}{1 - \beta_0 \frac{\alpha_s(m_Z)}{2\pi} \ln\left(\frac{m_Z}{x}\right)}. \quad (2.6)$$

Here $\alpha_s(m_Z) = 0.118$ and $\beta_0 = \frac{23}{3}$. The function $h(y, \hat{s}')$ in Eq. (2.2) is also defined by

$$h(y, \hat{s}') = -\frac{8}{9} \ln \frac{m_b}{\mu_b} - \frac{8}{9} \ln y + \frac{8}{27} + \frac{4}{9} x \quad (2.7)$$

$$-\frac{2}{9} (2+x) |1-x|^{1/2} \begin{cases} \left(\ln \left| \frac{\sqrt{1-x}+1}{\sqrt{1-x}-1} \right| - i\pi \right) & \text{for } x \equiv \frac{4z^2}{\hat{s}'} < 1 \\ 2 \arctan \frac{1}{\sqrt{x-1}} & \text{for } x \equiv \frac{4z^2}{\hat{s}'} > 1, \end{cases} \quad (2.8)$$

where $y = 1$ or $y = z = \frac{m_c}{m_b}$, and

$$h(0, \hat{s}') = \frac{8}{27} - \frac{8}{9} \ln \frac{m_b}{\mu_b} - \frac{4}{9} \ln \hat{s}' + \frac{4}{9} i\pi. \quad (2.9)$$

In Eq. (2.2), the remaining coefficients are given by [23]

$$C_j = \sum_{i=1}^8 k_{ji} \eta^{a_i} \quad (j = 1, \dots, 6), \quad (2.10)$$

where the k_{ji} are given as

$$\begin{aligned}
k_{1i} &= (0, 0, \frac{1}{2}, -\frac{1}{2}, 0, 0, 0, 0), \\
k_{2i} &= (0, 0, \frac{1}{2}, \frac{1}{2}, 0, 0, 0, 0), \\
k_{3i} &= (0, 0, -\frac{1}{14}, \frac{1}{6}, 0.0510, -0.1403, -0.0113, 0.0054), \\
k_{4i} &= (0, 0, -\frac{1}{14}, -\frac{1}{6}, 0.0984, 0.1214, 0.0156, 0.0026), \\
k_{5i} &= (0, 0, 0, 0, -0.0397, 0.0117, -0.0025, 0.0304), \\
k_{6i} &= (0, 0, 0, 0, 0.0335, 0.0239, -0.0462, -0.0112).
\end{aligned} \tag{2.11}$$

The explicit expression for the Wilson coefficient C_{10}^{SM} is given as

$$C_{10}^{\text{SM}} = -\frac{Y^{\text{SM}}}{\sin^2 \theta_W}. \tag{2.12}$$

Finally, the Wilson coefficient $C_7^{\text{eff,SM}}$ in the leading log approximation is defined by [21–24]

$$\begin{aligned}
C_7^{\text{eff,SM}}(\mu_b) &= \eta^{\frac{16}{23}} C_7(\mu_W) + \frac{8}{3} \left(\eta^{\frac{14}{23}} - \eta^{\frac{16}{23}} \right) C_8(\mu_W) \\
&+ C_2(\mu_W) \sum_{i=1}^8 h_i \eta^{a_i},
\end{aligned} \tag{2.13}$$

where

$$\eta = \frac{\alpha_s(\mu_W)}{\alpha_s(\mu_b)}, \tag{2.14}$$

and

$$\begin{aligned}
h_i &= (2.2996, -1.0880, -\frac{3}{7}, -\frac{1}{14}, -0.6494, -0.0380, -0.0186, -0.0057), \\
a_i &= (\frac{14}{23}, \frac{16}{23}, \frac{6}{23}, -\frac{12}{23}, 0.4086, -0.4230, -0.8994, 0.1456).
\end{aligned} \tag{2.18}$$

One of the most important new physics scenarios is SUSY. The different SUSY models involve the SUSY I, SUSY II, SUSY III and SUSY SO(10) scenarios according to the values of $\tan\beta$ and an extra parameter μ with the dimension of mass [25–28]. In SUSY I, the Wilson coefficient C_7^{eff} changes its sign, the μ takes a negative value, and the contributions of the neutral Higgs bosons (NHBs) have been disregarded. In the SUSY II model, the

$$\begin{aligned}
C_7(\mu_W) &= -\frac{1}{2} D_0^{\text{SM}}(x_t), & C_8(\mu_W) &= -\frac{1}{2} E_0^{\text{SM}}(x_t), \\
C_2(\mu_W) &= 1.
\end{aligned} \tag{2.15}$$

The functions $D_0^{\text{SM}}(x_t)$ and $E_0^{\text{SM}}(x_t)$, with $x_t = \frac{m_t^2}{m_W^2}$, are given by

$$D_0^{\text{SM}}(x_t) = -\frac{(8x_t^3 + 5x_t^2 - 7x_t)}{12(1-x_t)^3} + \frac{x_t^2(2-3x_t)}{2(1-x_t)^4} \ln x_t \tag{2.16}$$

and

$$E_0^{\text{SM}}(x_t) = -\frac{x_t(x_t^2 - 5x_t - 2)}{4(1-x_t)^3} + \frac{3x_t^2}{2(1-x_t)^4} \ln x_t. \tag{2.17}$$

The coefficients h_i and a_i inside $C_7^{\text{eff,SM}}$ are also given by [21,22]

value of the $\tan\beta$ is large and the masses of the superparticles are relatively small. In SUSY III, the $\tan\beta$ takes a large value and the masses of the superparticles are relatively large. In SUSY SO(10), the contributions of the NHBs are taken into account. The supersymmetric effective Hamiltonian in terms of the new operators coming from the NHBs exchanges diagrams, and the corresponding Wilson coefficients are written as

$$\begin{aligned}
\mathcal{H}_{\text{SUSY}}^{\text{eff}} &= \frac{G_F \alpha_{em} V_{tb} V_{ts}^*}{2\sqrt{2}\pi} \left[C_9^{\text{eff,SUSY}} \bar{s} \gamma_\mu (1 - \gamma_5) b \bar{\ell} \gamma^\mu \ell + C_9^{\text{eff,SUSY}} \bar{s} \gamma_\mu (1 + \gamma_5) b \bar{\ell} \gamma^\mu \ell + C_{10}^{\text{SUSY}} \bar{s} \gamma_\mu (1 - \gamma_5) b \bar{\ell} \gamma^\mu \gamma_5 \ell \right. \\
&+ C_{10}^{\text{SUSY}} \bar{s} \gamma_\mu (1 + \gamma_5) b \bar{\ell} \gamma^\mu \gamma_5 \ell - 2m_b C_7^{\text{eff,SUSY}} \frac{1}{q^2} \bar{s} i \sigma_{\mu\nu} q^\nu (1 + \gamma_5) b \bar{\ell} \gamma^\mu \ell - 2m_b C_7^{\text{eff,SUSY}} \frac{1}{q^2} \bar{s} i \sigma_{\mu\nu} q^\nu (1 - \gamma_5) b \bar{\ell} \gamma^\mu \ell \\
&\left. + C_{Q_1}^{\text{SUSY}} \bar{s} (1 + \gamma_5) b \bar{\ell} \ell + C_{Q_1}^{\text{SUSY}} \bar{s} (1 - \gamma_5) b \bar{\ell} \ell + C_{Q_2}^{\text{SUSY}} \bar{s} (1 + \gamma_5) b \bar{\ell} \gamma_5 \ell + C_{Q_2}^{\text{SUSY}} \bar{s} (1 - \gamma_5) b \bar{\ell} \gamma_5 \ell \right], \tag{2.19}
\end{aligned}$$

TABLE I. The Wilson coefficients in different SUSY models [26–29]. The values inside the parentheses are for the τ lepton.

Coefficient	SUSY I	SUSY II	SUSY III	SUSY SO(10)($A_0 = -1000$)
$C_7^{\text{eff,SUSY}}$	+0.376	+0.376	-0.376	-0.219
$C_9^{\text{eff,SUSY}}$	4.767	4.767	4.767	4.275
C_{10}^{SUSY}	-3.735	-3.735	-3.735	-4.732
$C_{Q_1}^{\text{SUSY}}$	0	6.5(16.5)	1.2(4.5)	$0.106 + 0i(1.775 + 0.002i)$
$C_{Q_2}^{\text{SUSY}}$	0	-6.5(-16.5)	-1.2(-4.5)	$-0.107 + 0i(-1.797 - 0.002i)$
$C_7^{\prime\text{eff,SUSY}}$	0	0	0	$0.039 + 0.038i$
$C_9^{\prime\text{eff,SUSY}}$	0	0	0	$0.011 + 0.072i$
$C_{10}^{\prime\text{SUSY}}$	0	0	0	$-0.075 - 0.67i$
$C_{Q_1}^{\prime\text{SUSY}}$	0	0	0	$-0.247 + 0.242i(-4.148 + 4.074i)$
$C_{Q_2}^{\prime\text{SUSY}}$	0	0	0	$-0.25 + 0.246i(-4.202 + 4.128i)$

where $C_9^{\text{eff,SUSY}}$, $C_9^{\prime\text{eff,SUSY}}$, C_{10}^{SUSY} , $C_{10}^{\prime\text{SUSY}}$, $C_7^{\text{eff,SUSY}}$, $C_7^{\prime\text{eff,SUSY}}$, $C_{Q_1}^{\text{SUSY}}$, $C_{Q_1}^{\prime\text{SUSY}}$, $C_{Q_2}^{\text{SUSY}}$, and $C_{Q_2}^{\prime\text{SUSY}}$ are the new Wilson coefficients in the different SUSY models. The new Wilson coefficients $C_{Q_1}^{(\prime)\text{SUSY}}$ and $C_{Q_2}^{(\prime)\text{SUSY}}$ come from NHBs exchanging [28]. The primed Wilson coefficients only appear in the SUSY SO(10) model. The values of Wilson coefficients in different supersymmetric models are presented in Table I [26–29].

The last new physics scenario which we consider in this work is the Randall-Sundrum scenario proposed to solve the gauge hierarchy and the flavor problems in 1999 [30,31]. It is a successful model, featuring one compact extra dimension with nonfactorizable anti-de Sitter (AdS₅) space-time [32]. This model describes the five-dimensional space-time manifold with coordinates (x ; y) and metric

$$ds^2 = e^{-2ky} \eta_{\mu\nu} dx^\mu dx^\nu - dy^2, \quad \eta_{\mu\nu} = \text{diag}(+1, -1, -1, -1). \quad (2.20)$$

The scale parameter k is defined as $k \simeq \mathcal{O}(M_{\text{Planck}})$. We choose it as $k = 10^{19}$ GeV. The fifth coordinate y varies in a range between two branes, 0 and L . $y = 0$ and $y = L$ correspond to the so-called UV brane and IR brane, respectively. The simplest RS model with only the SM gauge group in the bulk has many important problems with the electroweak precision parameters [33]. In the present work, we consider the RS model with an enlarged custodial protection based on $SU(3)_c \times SU(2)_L \times SU(2)_R \times U(1)_X \times P_{LR}$, where P_{LR} interchanges the two $SU(2)$ groups and is responsible for the protection of the $Z b_L \bar{b}_L$ vertex (for more information on the model, see Refs. [32–40]).

The effective Hamiltonian for the $b \rightarrow s \ell^+ \ell^-$ transition in the RS_c model is given as

$$\mathcal{H}_{\text{RS}_c}^{\text{eff}} = \frac{G_F \alpha_{em} V_{tb} V_{ts}^*}{2\sqrt{2}\pi} \left[C_9^{\text{eff,RS}_c} \bar{s} \gamma_\mu (1 - \gamma_5) b \bar{\ell} \gamma^\mu \ell + C_9^{\prime\text{eff,RS}_c} \bar{s} \gamma_\mu (1 + \gamma_5) b \bar{\ell} \gamma^\mu \ell + C_{10}^{\text{RS}_c} \bar{s} \gamma_\mu (1 - \gamma_5) b \bar{\ell} \gamma^\mu \gamma_5 \ell + C_{10}^{\prime\text{RS}_c} \bar{s} \gamma_\mu (1 + \gamma_5) b \bar{\ell} \gamma^\mu \gamma_5 \ell - 2m_b C_7^{\text{eff,RS}_c} \frac{1}{q^2} \bar{s} i \sigma_{\mu\nu} q^\nu (1 + \gamma_5) b \bar{\ell} \gamma^\mu \ell - 2m_b C_7^{\prime\text{eff,RS}_c} \frac{1}{q^2} \bar{s} i \sigma_{\mu\nu} q^\nu (1 - \gamma_5) b \bar{\ell} \gamma^\mu \ell \right], \quad (2.21)$$

where the new Wilson coefficients are modified considering the new interactions. The new coefficients in terms of the SM coefficients are written as [32–40]

$$C_i^{(\prime)\text{RS}_c} = C_i^{(\prime)\text{SM}} + \Delta C_i^{(\prime)}, \quad i = 7, 9, 10, \quad (2.22)$$

where

$$\begin{aligned} \Delta C_9 &= \left[\frac{\Delta Y_s}{\sin^2(\theta_w)} - 4\Delta Z_s \right], \\ \Delta C_9' &= \left[\frac{\Delta Y_s'}{\sin^2(\theta_w)} - 4\Delta Z_s' \right], \\ \Delta C_{10} &= -\frac{\Delta Y_s}{\sin^2(\theta_w)}, \end{aligned} \quad (2.23)$$

and

$$\Delta C'_{10} = -\frac{\Delta Y'_s}{\sin^2(\theta_w)}, \quad (2.24)$$

with

$$\begin{aligned} \Delta Y_s &= -\frac{1}{V_{tb}V_{ts}^*} \sum_X \frac{\Delta_L^{\ell\ell}(X) - \Delta_R^{\ell\ell}(X)}{4M_X^2 g_{\text{SM}}^2} \Delta_L^{bs}(X), \\ \Delta Y'_s &= -\frac{1}{V_{tb}V_{ts}^*} \sum_X \frac{\Delta_L^{\ell\ell}(X) - \Delta_R^{\ell\ell}(X)}{4M_X^2 g_{\text{SM}}^2} \Delta_R^{bs}(X), \\ \Delta Z_s &= \frac{1}{V_{tb}V_{ts}^*} \sum_X \frac{\Delta_R^{\ell\ell}(X)}{8M_X^2 g_{\text{SM}}^2 \sin^2(\theta_w)} \Delta_L^{bs}(X), \end{aligned} \quad (2.25)$$

and

$$\Delta Z'_s = \frac{1}{V_{tb}V_{ts}^*} \sum_X \frac{\Delta_R^{\ell\ell}(X)}{8M_X^2 g_{\text{SM}}^2 \sin^2(\theta_w)} \Delta_R^{bs}(X). \quad (2.26)$$

In the above equations, $X = Z, Z_H, Z',$ and $A^{(1)}$; $g_{\text{SM}}^2 = \frac{G_F}{\sqrt{2}} \frac{\alpha}{2\pi \sin^2(\theta_w)}$; and θ_w is the Weinberg angle. The functions inside $\Delta Y_s, \Delta Y'_s, \Delta Z_s,$ and $\Delta Z'_s$ are given in Refs. [32–40].

In the case of $\Delta C_7^{(\prime)}, \Delta C_7^{(\prime)}(\mu_b) = 0.429\Delta C_7^{(\prime)}(M_{KK}) + 0.128\Delta C_8^{(\prime)}(M_{KK})$ is used where the following three contributions are included [34]:

$$\begin{aligned} (\Delta C_7)_1 &= iQ_{ur} \sum_{F=u,c,t} [A + 2m_F^2(A' + B')] [\mathcal{D}_L^\dagger Y^u (Y^u)^\dagger Y^d \mathcal{D}_R]_{23}, \\ (\Delta C_7)_2 &= -iQ_{dr} \frac{8}{3} (g_s^{AD})^2 \sum_{F=d,s,b} [I_0 + A + B + 4m_F^2(I'_0 + A' + B')] [\mathcal{D}_L^\dagger \mathcal{R}_L Y^d \mathcal{R}_R \mathcal{D}_R]_{23}, \\ (\Delta C_7)_3 &= iQ_{dr} \frac{8}{3} (g_s^{AD})^2 \sum_{F=d,s,b} m_F [I_0 + A + B] \left\{ [\mathcal{D}_L^\dagger \mathcal{R}_L \mathcal{R}_L Y^d \mathcal{D}_R]_{23} + \frac{m_b}{m_s} [\mathcal{D}_L^\dagger Y^d \mathcal{R}_R \mathcal{R}_R \mathcal{D}_R]_{23} \right\}, \end{aligned} \quad (2.27)$$

$$\begin{aligned} (\Delta C'_7)_1 &= iQ_{ur} \sum_{F=u,c,t} [A + 2m_F^2(A' + B')] [\mathcal{D}_R^\dagger (Y^d)^\dagger Y^u (Y^u)^\dagger \mathcal{D}_L]_{23}, \\ (\Delta C'_7)_2 &= -iQ_{dr} \frac{8}{3} (g_s^{AD})^2 \sum_{F=d,s,b} [I_0 + A + B + 4m_F^2(I'_0 + A' + B')] [\mathcal{D}_R^\dagger \mathcal{R}_R (Y^d)^\dagger \mathcal{R}_L \mathcal{D}_L]_{23}, \\ (\Delta C'_7)_3 &= iQ_{dr} \frac{8}{3} (g_s^{AD})^2 \sum_{F=d,s,b} m_F [I_0 + A + B] \left\{ [\mathcal{D}_R^\dagger \mathcal{R}_R \mathcal{R}_R (Y^d)^\dagger \mathcal{D}_L]_{23} + \frac{m_b}{m_s} [\mathcal{D}_R^\dagger (Y^d)^\dagger \mathcal{R}_L \mathcal{R}_L \mathcal{D}_L]_{23} \right\}, \end{aligned} \quad (2.28)$$

$$\begin{aligned} (\Delta C_8)_1 &= ir \sum_{F=u,c,t} [A + 2m_F^2(A' + B')] [\mathcal{D}_L^\dagger Y^u (Y^u)^\dagger Y^d \mathcal{D}_R]_{23}, \\ (\Delta C_8)_2 &= -ir \frac{9}{8} (g_s^{AD})^2 \frac{v^2}{m_b m_s} \mathcal{T}_3 \sum_{F=d,s,b} [\bar{A} + \bar{B} + 2m_F^2(\bar{A}' + \bar{B}')] [\mathcal{D}_L^\dagger Y^d \mathcal{R}_R (Y^d)^\dagger \mathcal{R}_L Y^d \mathcal{D}_R]_{23}, \\ (\Delta C_8)_3 &= -ir \frac{9}{4} (g_s^{AD})^2 \mathcal{T}_3 \sum_{F=d,s,b} [\bar{A} + \bar{B} + 2m_F^2(\bar{A}' + \bar{B}')] [\mathcal{D}_L^\dagger \mathcal{R}_L Y^d \mathcal{R}_R \mathcal{D}_R]_{23}, \end{aligned} \quad (2.29)$$

$$\begin{aligned} (\Delta C'_8)_1 &= ir \sum_{F=u,c,t} [A + 2m_F^2(A' + B')] [\mathcal{D}_R^\dagger (Y^d)^\dagger Y^u (Y^u)^\dagger \mathcal{D}_L]_{23}, \\ (\Delta C'_8)_2 &= -ir \frac{9}{8} (g_s^{AD})^2 \frac{v^2}{m_b m_s} \mathcal{T}_3 \sum_{F=d,s,b} [\bar{A} + \bar{B} + 2m_F^2(\bar{A}' + \bar{B}')] [\mathcal{D}_R^\dagger (Y^d)^\dagger \mathcal{R}_L Y^d \mathcal{R}_R (Y^d)^\dagger \mathcal{D}_L]_{23}, \\ (\Delta C'_8)_3 &= -ir \frac{9}{4} (g_s^{AD})^2 \mathcal{T}_3 \sum_{F=d,s,b} [\bar{A} + \bar{B} + 2m_F^2(\bar{A}' + \bar{B}')] [\mathcal{D}_R^\dagger \mathcal{R}_R (Y^d)^\dagger \mathcal{R}_L \mathcal{D}_L]_{23}, \end{aligned} \quad (2.30)$$

where $r = \frac{v}{4s_w^2 V_{tb} V_{ts}^* m_b}$ and $\mathcal{T}_3 = \frac{1}{L} \int_0^L dy [g(y)]^2$. For the parameters inside the above equations and the related diagrams, see Refs. [32–40]. Q_u and Q_d represent the electric charges of the up- and down-type quarks, respectively. The functions $I_0^{(\prime)}, A^{(\prime)},$ and $B^{(\prime)}$ are given as

TABLE II. The values of modifications in Wilson coefficients in the RS_c model used in the analysis [34].

	ΔC_7	$\Delta C'_7$	ΔC_9	$\Delta C'_9$	ΔC_{10}	$\Delta C'_{10}$
Values	0.046	0.05	0.0023	0.038	0.030	0.50

$$\begin{aligned}
I_0(t) &= \frac{i}{(4\pi)^2} \frac{1}{M_{KK}^2} \left(-\frac{1}{t-1} + \frac{\ln(t)}{(t-1)^2} \right), \\
I'_0(t) &= \frac{i}{(4\pi)^2} \frac{1}{M_{KK}^4} \left(\frac{1+t}{2t(t-1)^2} - \frac{\ln(t)}{(t-1)^3} \right), \\
A(t) = B(t) &= \frac{i}{(4\pi)^2} \frac{1}{4M_{KK}^2} \left(\frac{t-3}{(t-1)^2} + \frac{2\ln(t)}{(t-1)^3} \right), \\
A'(t) = 2B'(t) &= \frac{i}{(4\pi)^2} \frac{1}{M_{KK}^4} \left(-\frac{t^2-5t-2}{6t(t-1)^3} - \frac{\ln(t)}{(t-1)^4} \right), \\
\bar{A}(t) = \bar{B}(t) &= \frac{i}{(4\pi)^2} \frac{1}{4M_{KK}^2} \left(-\frac{3t-1}{(t-1)^2} + \frac{2t^2\ln(t)}{(t-1)^3} \right), \\
\bar{A}'(t) = \bar{B}'(t) &= \frac{i}{(4\pi)^2} \frac{1}{4M_{KK}^4} \left(\frac{5t+1}{(t-1)^3} - \frac{2t(2+t)\ln(t)}{(t-1)^4} \right),
\end{aligned} \tag{2.31}$$

with $t = m_F^2/M_{KK}^2$ (for more information, see Ref. [34]).

Fitting the parameters to the $B \rightarrow K^* \mu^+ \mu^-$ channel, the modifications on Wilson coefficients in the RS_c model are found in Table II [34].

B. Transition amplitude and matrix elements

The amplitude of the transition under consideration is obtained by sandwiching the corresponding effective Hamiltonian between the initial and final baryonic states, i.e.,

$$\mathcal{M}^{\Lambda_b \rightarrow \Lambda \ell^+ \ell^-} = \langle \Lambda(p_\Lambda) | \mathcal{H}^{\text{eff}} | \Lambda_b(p_{\Lambda_b}) \rangle, \tag{2.32}$$

where p_{Λ_b} and p_Λ are momenta of the initial and final baryons. To calculate the amplitude, we need to know the following matrix elements, which are parametrized in terms of 12 form factors in full QCD:

$$\begin{aligned}
\langle \Lambda(p_\Lambda) | \bar{s} \gamma_\mu (1 - \gamma_5) b | \Lambda_b(p_{\Lambda_b}) \rangle &= \bar{u}_\Lambda(p_\Lambda) [\gamma_\mu f_1(q^2) + i \sigma_{\mu\nu} q^\nu f_2(q^2) + q^\mu f_3(q^2) \\
&\quad - \gamma_\mu \gamma_5 g_1(q^2) - i \sigma_{\mu\nu} \gamma_5 q^\nu g_2(q^2) - q^\mu \gamma_5 g_3(q^2)] u_{\Lambda_b}(p_{\Lambda_b}),
\end{aligned} \tag{2.33}$$

$$\begin{aligned}
\langle \Lambda(p_\Lambda) | \bar{s} \gamma_\mu (1 + \gamma_5) b | \Lambda_b(p_{\Lambda_b}) \rangle &= \bar{u}_\Lambda(p_\Lambda) [\gamma_\mu f_1(q^2) + i \sigma_{\mu\nu} q^\nu f_2(q^2) + q^\mu f_3(q^2) \\
&\quad + \gamma_\mu \gamma_5 g_1(q^2) + i \sigma_{\mu\nu} \gamma_5 q^\nu g_2(q^2) + q^\mu \gamma_5 g_3(q^2)] u_{\Lambda_b}(p_{\Lambda_b}),
\end{aligned} \tag{2.34}$$

$$\begin{aligned}
\langle \Lambda(p_\Lambda) | \bar{s} i \sigma_{\mu\nu} q^\nu (1 + \gamma_5) b | \Lambda_b(p_{\Lambda_b}) \rangle &= \bar{u}_\Lambda(p_\Lambda) [\gamma_\mu f_1^T(q^2) + i \sigma_{\mu\nu} q^\nu f_2^T(q^2) + q^\mu f_3^T(q^2) \\
&\quad + \gamma_\mu \gamma_5 g_1^T(q^2) + i \sigma_{\mu\nu} \gamma_5 q^\nu g_2^T(q^2) + q^\mu \gamma_5 g_3^T(q^2)] u_{\Lambda_b}(p_{\Lambda_b}),
\end{aligned} \tag{2.35}$$

$$\begin{aligned}
\langle \Lambda(p_\Lambda) | \bar{s} i \sigma_{\mu\nu} q^\nu (1 - \gamma_5) b | \Lambda_b(p_{\Lambda_b}) \rangle &= \bar{u}_\Lambda(p_\Lambda) [\gamma_\mu f_1^T(q^2) + i \sigma_{\mu\nu} q^\nu f_2^T(q^2) + q^\mu f_3^T(q^2) \\
&\quad - \gamma_\mu \gamma_5 g_1^T(q^2) - i \sigma_{\mu\nu} \gamma_5 q^\nu g_2^T(q^2) - q^\mu \gamma_5 g_3^T(q^2)] u_{\Lambda_b}(p_{\Lambda_b}),
\end{aligned} \tag{2.36}$$

$$\begin{aligned}
\langle \Lambda(p_\Lambda) | \bar{s} (1 + \gamma_5) b | \Lambda_b(p_{\Lambda_b}) \rangle &= \frac{1}{m_b} \bar{u}_\Lambda(p_\Lambda) [q f_1(q^2) + i q^\mu \sigma_{\mu\nu} q^\nu f_2(q^2) + q^2 f_3(q^2) \\
&\quad - q \gamma_5 g_1(q^2) - i q^\mu \sigma_{\mu\nu} \gamma_5 q^\nu g_2(q^2) - q^2 \gamma_5 g_3(q^2)] u_{\Lambda_b}(p_{\Lambda_b}),
\end{aligned} \tag{2.37}$$

and

$$\begin{aligned} \langle \Lambda(p_\Lambda) | \bar{s}(1 - \gamma_5) b | \Lambda_b(p_{\Lambda_b}) \rangle &= \frac{1}{m_b} \bar{u}_\Lambda(p_\Lambda) [q f_1(q^2) + i q^\mu \sigma_{\mu\nu} q^\nu f_2(q^2) + q^2 f_3(q^2) \\ &\quad + q \gamma_5 g_1(q^2) + i q^\mu \sigma_{\mu\nu} \gamma_5 q^\nu g_2(q^2) + q^2 \gamma_5 g_3(q^2)] u_{\Lambda_b}(p_{\Lambda_b}), \end{aligned} \quad (2.38)$$

where $f_i^{(T)}$ and $g_i^{(T)}$ (with i running from 1 to 3) are transition form factors, and u_{Λ_b} and u_Λ are spinors of the Λ_b and Λ baryons, respectively. We will use these form factors from Ref. [19] that have been calculated using the light-cone QCD sum rules.

Using the above transition matrix elements in terms of form factors, we find the amplitude of the transition under consideration in different scenarios. In the SM, we find

$$\begin{aligned} \mathcal{M}_{\text{SM}}^{\Lambda_b \rightarrow \Lambda \ell^+ \ell^-} &= \frac{G_F \alpha_{em} V_{tb} V_{ts}^*}{2\sqrt{2}\pi} \{ [\bar{u}_\Lambda(p_\Lambda) (\gamma_\mu [\mathcal{A}_1^{\text{SM}} R + \mathcal{B}_1^{\text{SM}} L] + i \sigma_{\mu\nu} q^\nu [\mathcal{A}_2^{\text{SM}} R + \mathcal{B}_2^{\text{SM}} L] + q^\mu [\mathcal{A}_3^{\text{SM}} R + \mathcal{B}_3^{\text{SM}} L]) u_{\Lambda_b}(p_{\Lambda_b})] (\bar{\ell} \gamma^\mu \ell) \\ &\quad + [\bar{u}_\Lambda(p_\Lambda) (\gamma_\mu [\mathcal{D}_1^{\text{SM}} R + \mathcal{E}_1^{\text{SM}} L] + i \sigma_{\mu\nu} q^\nu [\mathcal{D}_2^{\text{SM}} R + \mathcal{E}_2^{\text{SM}} L] + q^\mu [\mathcal{D}_3^{\text{SM}} R + \mathcal{E}_3^{\text{SM}} L]) u_{\Lambda_b}(p_{\Lambda_b})] (\bar{\ell} \gamma^\mu \gamma_5 \ell) \}. \end{aligned} \quad (2.39)$$

In the case of SUSY we get

$$\begin{aligned} \mathcal{M}_{\text{SUSY}}^{\Lambda_b \rightarrow \Lambda \ell^+ \ell^-} &= \frac{G_F \alpha_{em} V_{tb} V_{ts}^*}{2\sqrt{2}\pi} \{ [\bar{u}_\Lambda(p_\Lambda) (\gamma_\mu [\mathcal{A}_1^{\text{SUSY}} R + \mathcal{B}_1^{\text{SUSY}} L] + i \sigma_{\mu\nu} q^\nu [\mathcal{A}_2^{\text{SUSY}} R + \mathcal{B}_2^{\text{SUSY}} L] \\ &\quad + q^\mu [\mathcal{A}_3^{\text{SUSY}} R + \mathcal{B}_3^{\text{SUSY}} L]) u_{\Lambda_b}(p_{\Lambda_b})] (\bar{\ell} \gamma^\mu \ell) + [\bar{u}_\Lambda(p_\Lambda) (\gamma_\mu [\mathcal{D}_1^{\text{SUSY}} R + \mathcal{E}_1^{\text{SUSY}} L] + i \sigma_{\mu\nu} q^\nu [\mathcal{D}_2^{\text{SUSY}} R + \mathcal{E}_2^{\text{SUSY}} L] \\ &\quad + q^\mu [\mathcal{D}_3^{\text{SUSY}} R + \mathcal{E}_3^{\text{SUSY}} L]) u_{\Lambda_b}(p_{\Lambda_b})] (\bar{\ell} \gamma^\mu \gamma_5 \ell) + [\bar{u}_\Lambda(p_\Lambda) (q [\mathcal{G}_1^{\text{SUSY}} R + \mathcal{H}_1^{\text{SUSY}} L] \\ &\quad + i q^\mu \sigma_{\mu\nu} q^\nu [\mathcal{G}_2^{\text{SUSY}} R + \mathcal{H}_2^{\text{SUSY}} L] + q^2 [\mathcal{G}_3^{\text{SUSY}} R + \mathcal{H}_3^{\text{SUSY}} L]) u_{\Lambda_b}(p_{\Lambda_b})] (\bar{\ell} \ell) + [\bar{u}_\Lambda(p_\Lambda) (q [\mathcal{K}_1^{\text{SUSY}} R + \mathcal{S}_1^{\text{SUSY}} L] \\ &\quad + i q^\mu \sigma_{\mu\nu} q^\nu [\mathcal{K}_2^{\text{SUSY}} R + \mathcal{S}_2^{\text{SUSY}} L] + q^2 [\mathcal{K}_3^{\text{SUSY}} R + \mathcal{S}_3^{\text{SUSY}} L]) u_{\Lambda_b}(p_{\Lambda_b})] (\bar{\ell} \gamma_5 \ell) \}, \end{aligned} \quad (2.40)$$

and for RS_c we obtain

$$\begin{aligned} \mathcal{M}_{\text{RS}_c}^{\Lambda_b \rightarrow \Lambda \ell^+ \ell^-} &= \frac{G_F \alpha_{em} V_{tb} V_{ts}^*}{2\sqrt{2}\pi} \{ [\bar{u}_\Lambda(p_\Lambda) (\gamma_\mu [\mathcal{A}_1^{\text{RS}_c} R + \mathcal{B}_1^{\text{RS}_c} L] + i \sigma_{\mu\nu} q^\nu [\mathcal{A}_2^{\text{RS}_c} R + \mathcal{B}_2^{\text{RS}_c} L] \\ &\quad + q^\mu [\mathcal{A}_3^{\text{RS}_c} R + \mathcal{B}_3^{\text{RS}_c} L]) u_{\Lambda_b}(p_{\Lambda_b})] (\bar{\ell} \gamma^\mu \ell) + [\bar{u}_\Lambda(p_\Lambda) (\gamma_\mu [\mathcal{D}_1^{\text{RS}_c} R + \mathcal{E}_1^{\text{RS}_c} L] + i \sigma_{\mu\nu} q^\nu [\mathcal{D}_2^{\text{RS}_c} R + \mathcal{E}_2^{\text{RS}_c} L] \\ &\quad + q^\mu [\mathcal{D}_3^{\text{RS}_c} R + \mathcal{E}_3^{\text{RS}_c} L]) u_{\Lambda_b}(p_{\Lambda_b})] (\bar{\ell} \gamma^\mu \gamma_5 \ell) \}, \end{aligned} \quad (2.41)$$

where $R = (1 + \gamma_5)/2$ and $L = (1 - \gamma_5)/2$ are the right-handed and left-handed projectors, respectively. In the above equations, the calligraphic coefficients are defined in different models as

$$\begin{aligned} \mathcal{A}_1 &= f_1 C_9^{\text{eff}+} - g_1 C_9^{\text{eff}-} - 2m_b \frac{1}{q^2} [f_1^T C_7^{\text{eff}+} + g_1^T C_7^{\text{eff}-}], & \mathcal{A}_2 &= \mathcal{A}_1(1 \rightarrow 2), & \mathcal{A}_3 &= \mathcal{A}_1(1 \rightarrow 3), \\ \mathcal{B}_1 &= f_1 C_9^{\text{eff}+} + g_1 C_9^{\text{eff}f-} - 2m_b \frac{1}{q^2} [f_1^T C_7^{\text{eff}+} - g_1^T C_7^{\text{eff}-}], & \mathcal{B}_2 &= \mathcal{B}_1(1 \rightarrow 2), & \mathcal{B}_3 &= \mathcal{B}_1(1 \rightarrow 3), \\ \mathcal{D}_1 &= f_1 C_{10}^+ - g_1 C_{10}^-, & \mathcal{D}_2 &= \mathcal{D}_1(1 \rightarrow 2), & \mathcal{D}_3 &= \mathcal{D}_1(1 \rightarrow 3), \\ \mathcal{E}_1 &= f_1 C_{10}^+ + g_1 C_{10}^-, & \mathcal{E}_2 &= \mathcal{E}_1(1 \rightarrow 2), & \mathcal{E}_3 &= \mathcal{E}_1(1 \rightarrow 3), \\ \mathcal{G}_1 &= \frac{1}{m_b} [f_1 C_{Q_1}^+ - g_1 C_{Q_1}^-], & \mathcal{G}_2 &= \mathcal{G}_1(1 \rightarrow 2), & \mathcal{G}_3 &= \mathcal{G}_1(1 \rightarrow 3), \\ \mathcal{H}_1 &= \frac{1}{m_b} [f_1 C_{Q_1}^+ + g_1 C_{Q_1}^-], & \mathcal{H}_2 &= \mathcal{H}_1(1 \rightarrow 2), & \mathcal{H}_3 &= \mathcal{H}_1(1 \rightarrow 3), \\ \mathcal{K}_1 &= \frac{1}{m_b} [f_1 C_{Q_2}^+ - g_1 C_{Q_2}^-], & \mathcal{K}_2 &= \mathcal{K}_1(1 \rightarrow 2), & \mathcal{K}_3 &= \mathcal{K}_1(1 \rightarrow 3), \\ \mathcal{S}_1 &= \frac{1}{m_b} [f_1 C_{Q_2}^+ + g_1 C_{Q_2}^-], & \mathcal{S}_2 &= \mathcal{S}_1(1 \rightarrow 2), & \mathcal{S}_3 &= \mathcal{S}_1(1 \rightarrow 3), \end{aligned} \quad (2.42)$$

with

$$\begin{aligned}
C_9^{\text{eff}+} &= C_9^{\text{eff}} + C_9^{\prime\text{eff}}, & C_9^{\text{eff}-} &= C_9^{\text{eff}} - C_9^{\prime\text{eff}}, & C_7^{\text{eff}+} &= C_7^{\text{eff}} + C_7^{\prime\text{eff}}, & C_7^{\text{eff}-} &= C_7^{\text{eff}} - C_7^{\prime\text{eff}}, & C_{10}^+ &= C_{10} + C'_{10}, \\
C_{10}^- &= C_{10} - C'_{10}, & C_{Q_1}^+ &= C_{Q_1} + C'_{Q_1}, & C_{Q_1}^- &= C_{Q_1} - C'_{Q_1}, & C_{Q_2}^+ &= C_{Q_2} + C'_{Q_2}, & C_{Q_2}^- &= C_{Q_2} - C'_{Q_2}.
\end{aligned} \tag{2.43}$$

III. PHYSICAL OBSERVABLES

A. The differential decay width

In the present subsection, we would like to calculate the differential decay width for the decay channel under consideration. Using the decay amplitude and the transition matrix elements in terms of form factors, the supersymmetric differential decay rate, as the most comprehensive differential decay rate among the models under consideration, is obtained as

$$\frac{d^2\Gamma^{\text{SUSY}}}{d\hat{s}dz}(z, \hat{s}) = \frac{G_F^2 \alpha_{em}^2 m_{\Lambda_b}}{16384\pi^5} |V_{tb} V_{ts}^*|^2 v \sqrt{\lambda(1, r, \hat{s})} [\mathcal{T}_0^{\text{SUSY}}(\hat{s}) + \mathcal{T}_1^{\text{SUSY}}(\hat{s})z + \mathcal{T}_2^{\text{SUSY}}(\hat{s})z^2], \tag{3.1}$$

where $z = \cos \theta$, with θ being the angle between the momenta of the lepton l^+ and the Λ_b in the center of mass of leptons, $v = \sqrt{1 - \frac{4m_\ell^2}{q^2}}$ is the lepton velocity, $\lambda = \lambda(1, r, \hat{s}) = (1 - r - \hat{s})^2 - 4r\hat{s}$ is the usual triangle function, $\hat{s} = q^2/m_{\Lambda_b}^2$, and $r = m_\Lambda^2/m_{\Lambda_b}^2$. The functions $\mathcal{T}_0^{\text{SUSY}}(\hat{s})$, $\mathcal{T}_1^{\text{SUSY}}(\hat{s})$, and $\mathcal{T}_2^{\text{SUSY}}(\hat{s})$ are obtained as

$$\begin{aligned}
\mathcal{T}_0^{\text{SUSY}}(\hat{s}) &= 32m_\ell^2 m_{\Lambda_b}^4 \hat{s} (1 + r - \hat{s}) (|\mathcal{D}_3|^2 + |\mathcal{E}_3|^2) + 64m_\ell^2 m_{\Lambda_b}^3 (1 - r - \hat{s}) \text{Re}[\mathcal{D}_1^* \mathcal{E}_3 + \mathcal{D}_3 \mathcal{E}_1^*] \\
&+ 64m_{\Lambda_b}^2 \sqrt{r} (6m_\ell^2 - m_{\Lambda_b}^2 \hat{s}) \text{Re}[\mathcal{D}_1^* \mathcal{E}_1] + 64m_\ell^2 m_{\Lambda_b}^3 \sqrt{r} \{2m_{\Lambda_b} \hat{s} \text{Re}[\mathcal{D}_3^* \mathcal{E}_3] + (1 - r + \hat{s}) \text{Re}[\mathcal{D}_1^* \mathcal{D}_3 + \mathcal{E}_1^* \mathcal{E}_3]\} \\
&+ 32m_{\Lambda_b}^2 (2m_\ell^2 + m_{\Lambda_b}^2 \hat{s}) \{(1 - r + \hat{s}) m_{\Lambda_b} \sqrt{r} \text{Re}[\mathcal{A}_1^* \mathcal{A}_2 + \mathcal{B}_1^* \mathcal{B}_2] \\
&- m_{\Lambda_b} (1 - r - \hat{s}) \text{Re}[\mathcal{A}_1^* \mathcal{B}_2 + \mathcal{A}_2^* \mathcal{B}_1] - 2\sqrt{r} (\text{Re}[\mathcal{A}_1^* \mathcal{B}_1] + m_{\Lambda_b}^2 \hat{s} \text{Re}[\mathcal{A}_2^* \mathcal{B}_2])\} \\
&+ 8m_{\Lambda_b}^2 \{4m_\ell^2 (1 + r - \hat{s}) + m_{\Lambda_b}^2 [(1 - r)^2 - \hat{s}^2]\} (|\mathcal{A}_1|^2 + |\mathcal{B}_1|^2) \\
&+ 8m_{\Lambda_b}^4 \{4m_\ell^2 [\lambda + (1 + r - \hat{s}) \hat{s}] + m_{\Lambda_b}^2 \hat{s} [(1 - r)^2 - \hat{s}^2]\} (|\mathcal{A}_2|^2 + |\mathcal{B}_2|^2) \\
&- 8m_{\Lambda_b}^2 \{4m_\ell^2 (1 + r - \hat{s}) - m_{\Lambda_b}^2 [(1 - r)^2 - \hat{s}^2]\} (|\mathcal{D}_1|^2 + |\mathcal{E}_1|^2) \\
&+ 8m_{\Lambda_b}^5 \hat{s} v^2 \{-8m_{\Lambda_b} \hat{s} \sqrt{r} \text{Re}[\mathcal{D}_2^* \mathcal{E}_2] + 4(1 - r + \hat{s}) \sqrt{r} \text{Re}[\mathcal{D}_1^* \mathcal{D}_2 + \mathcal{E}_1^* \mathcal{E}_2] \\
&- 4(1 - r - \hat{s}) \text{Re}[\mathcal{D}_1^* \mathcal{E}_2 + \mathcal{D}_2^* \mathcal{E}_1] + m_{\Lambda_b} [(1 - r)^2 - \hat{s}^2] (|\mathcal{D}_2|^2 + |\mathcal{E}_2|^2)\} \\
&- 8m_{\Lambda_b}^4 \{4m_\ell [(1 - r)^2 - \hat{s}(1 + r)] \text{Re}[\mathcal{D}_1^* \mathcal{K}_1 + \mathcal{E}_1^* \mathcal{S}_1] + (4m_\ell^2 - m_{\Lambda_b}^2 \hat{s}) [(1 - r)^2 - \hat{s}(1 + r)] (|\mathcal{G}_1|^2 + |\mathcal{H}_1|^2) \\
&+ 4m_{\Lambda_b}^2 \sqrt{r} \hat{s}^2 (4m_\ell^2 - m_{\Lambda_b}^2 \hat{s}) \text{Re}[\mathcal{G}_3^* \mathcal{H}_3]\} - 8m_{\Lambda_b}^5 \hat{s} \{2\sqrt{r} (4m_\ell^2 - m_{\Lambda_b}^2 \hat{s}) (1 - r + \hat{s}) \text{Re}[\mathcal{G}_1^* \mathcal{G}_3 + \mathcal{H}_1^* \mathcal{H}_3] \\
&+ 4m_\ell \sqrt{r} (1 - r + \hat{s}) \text{Re}[\mathcal{D}_1^* \mathcal{K}_3 + \mathcal{E}_1^* \mathcal{S}_3 + \mathcal{D}_3^* \mathcal{K}_1 + \mathcal{E}_3^* \mathcal{S}_1] + 4m_\ell (1 - r - \hat{s}) \text{Re}[\mathcal{D}_1^* \mathcal{S}_3 + \mathcal{E}_1^* \mathcal{K}_3 + \mathcal{D}_3^* \mathcal{S}_1 + \mathcal{E}_3^* \mathcal{K}_1] \\
&+ 2(1 - r - \hat{s}) (4m_\ell^2 - m_{\Lambda_b}^2 \hat{s}) \text{Re}[\mathcal{G}_1^* \mathcal{H}_3 + \mathcal{H}_1^* \mathcal{G}_3] - m_{\Lambda_b} [(1 - r)^2 - \hat{s}(1 + r)] (|\mathcal{K}_1|^2 + |\mathcal{S}_1|^2)\} \\
&- 32m_{\Lambda_b}^4 \sqrt{r} \hat{s} \{2m_\ell \text{Re}[\mathcal{D}_1^* \mathcal{S}_1 + \mathcal{E}_1^* \mathcal{K}_1] + (4m_\ell^2 - m_{\Lambda_b}^2 \hat{s}) \text{Re}[\mathcal{G}_1^* \mathcal{H}_1]\} \\
&+ 8m_{\Lambda_b}^6 \hat{s}^2 \{4\sqrt{r} \text{Re}[\mathcal{K}_1^* \mathcal{S}_1] + 2m_{\Lambda_b} \sqrt{r} (1 - r + \hat{s}) \text{Re}[\mathcal{K}_1^* \mathcal{K}_3 + \mathcal{S}_1^* \mathcal{S}_3] + 2m_{\Lambda_b} (1 - r - \hat{s}) \text{Re}[\mathcal{K}_1^* \mathcal{S}_3 + \mathcal{S}_1^* \mathcal{K}_3] \\
&- (4m_\ell^2 - m_{\Lambda_b}^2 \hat{s}) (1 + r - \hat{s}) (|\mathcal{G}_3|^2 + |\mathcal{H}_3|^2) - 4m_\ell (1 + r - \hat{s}) \text{Re}[\mathcal{D}_3^* \mathcal{K}_3 + \mathcal{E}_3^* \mathcal{S}_3] - 8m_\ell \sqrt{r} \text{Re}[\mathcal{D}_3^* \mathcal{S}_3 + \mathcal{E}_3^* \mathcal{K}_3]\} \\
&+ 8m_{\Lambda_b}^8 \hat{s}^3 \{(1 + r - \hat{s}) (|\mathcal{K}_3|^2 + |\mathcal{S}_3|^2) + 4\sqrt{r} \text{Re}[\mathcal{K}_3^* \mathcal{S}_3]\}, \tag{3.2}
\end{aligned}$$

$$\begin{aligned}
\mathcal{T}_1^{\text{SUSY}}(\hat{s}) &= -32m_{\Lambda_b}^4 m_\ell \sqrt{\lambda} v (1 - r) \text{Re}(\mathcal{A}_1^* \mathcal{G}_1 + \mathcal{B}_1^* \mathcal{H}_1) - 16m_{\Lambda_b}^4 \hat{s} v \sqrt{\lambda} \{2\text{Re}(\mathcal{A}_1^* \mathcal{D}_1) - 2\text{Re}(\mathcal{B}_1^* \mathcal{E}_1) \\
&+ 2m_{\Lambda_b} \text{Re}(\mathcal{B}_1^* \mathcal{D}_2 - \mathcal{B}_2^* \mathcal{D}_1 + \mathcal{A}_2^* \mathcal{E}_1 - \mathcal{A}_1^* \mathcal{E}_2) + 2m_{\Lambda_b} m_\ell \text{Re}(\mathcal{A}_1^* \mathcal{H}_3 + \mathcal{B}_1^* \mathcal{G}_3 - \mathcal{A}_2^* \mathcal{H}_1 - \mathcal{B}_2^* \mathcal{G}_1)\} \\
&+ 32m_{\Lambda_b}^5 \hat{s} v \sqrt{\lambda} \{m_{\Lambda_b} (1 - r) \text{Re}(\mathcal{A}_2^* \mathcal{D}_2 - \mathcal{B}_2^* \mathcal{E}_2) + \sqrt{r} \text{Re}(\mathcal{A}_2^* \mathcal{D}_1 + \mathcal{A}_1^* \mathcal{D}_2 - \mathcal{B}_2^* \mathcal{E}_1 - \mathcal{B}_1^* \mathcal{E}_2) \\
&- \sqrt{r} m_\ell \text{Re}(\mathcal{A}_1^* \mathcal{G}_3 + \mathcal{B}_1^* \mathcal{H}_3 + \mathcal{A}_2^* \mathcal{G}_1 + \mathcal{B}_2^* \mathcal{H}_1)\} + 32m_{\Lambda_b}^6 m_\ell \sqrt{\lambda} v \hat{s}^2 \text{Re}(\mathcal{A}_2^* \mathcal{G}_3 + \mathcal{B}_2^* \mathcal{H}_3), \tag{3.3}
\end{aligned}$$

and

$$\begin{aligned} \mathcal{T}_2^{\text{SUSY}}(\hat{s}) = & -8m_{\Lambda_b}^4 v^2 \lambda (|\mathcal{A}_1|^2 + |\mathcal{B}_1|^2 + |\mathcal{D}_1|^2 + |\mathcal{E}_1|^2) \\ & + 8m_{\Lambda_b}^6 \hat{s} v^2 \lambda (|\mathcal{A}_2|^2 + |\mathcal{B}_2|^2 + |\mathcal{D}_2|^2 + |\mathcal{E}_2|^2). \end{aligned} \quad (3.4)$$

Integrating Eq. (3.1) over z in the interval $[-1, 1]$, we obtain the differential decay width only in terms of \hat{s} as

$$\begin{aligned} \frac{d\Gamma^{\text{SUSY}}}{d\hat{s}}(\hat{s}) = & \frac{G_F^2 \alpha_{em}^2 m_{\Lambda_b}}{8192\pi^5} |V_{tb} V_{ts}^*|^2 v \sqrt{\lambda} \\ & \times \left[\mathcal{T}_0^{\text{SUSY}}(\hat{s}) + \frac{1}{3} \mathcal{T}_2^{\text{SUSY}}(\hat{s}) \right]. \end{aligned} \quad (3.5)$$

The differential decay rate of RS_c is found from $\frac{d\Gamma^{\text{SUSY}}}{d\hat{s}}(\hat{s})$ by replacing C_{Q_1} , C'_{Q_1} , C_{Q_2} and C'_{Q_2} with zero. In the case of SM, $\frac{d\Gamma^{\text{SM}}}{d\hat{s}}(\hat{s})$ is found from the supersymmetric differential decay rate via setting C_7^{eff} , C_9^{eff} , C_{10} , C_{Q_1} , C'_{Q_1} , C_{Q_2} , and C'_{Q_2} to zero.

B. The differential branching ratio

In this subsection, we numerically analyze the differential branching ratio that depends on q^2 for the $\Lambda_b \rightarrow \Lambda \ell^+ \ell^-$ decay in SMLCSR, SUSY, and RS_c scenarios. In order to discuss the variation of the differential branching ratio with respect to q^2 , we shall present some values of input parameters in Table III besides the form factors as the main inputs.

By using all these input parameters and the form factors with their uncertainties, we present the dependence of the differential branching ratio of the $\Lambda_b \rightarrow \Lambda \ell^+ \ell^-$ on q^2 in SMLCSR, RS_c and different SUSY models in Figs. 1–6. In these figures we also show the experimental data provided

TABLE III. The values of some input parameters used in our calculations, taken generally from PDG [41].

Input parameters	Values
m_μ	0.10565 GeV
m_τ	1.77682 GeV
m_c	1.275 ± 0.025 GeV
m_b	4.18 ± 0.03 GeV
m_t	$173.21 \pm 0.51 \pm 0.71$ GeV
m_W	80.385 ± 0.015 GeV
m_{Λ_b}	5.6195 ± 0.0004 GeV
m_Λ	1.11568 GeV
τ_{Λ_b}	$(1.451 \pm 0.013) \times 10^{-12}$ s
\hbar	6.582×10^{-25} GeV s
G_F	1.166×10^{-5} GeV ⁻²
α_{em}	1/137
$ V_{tb} V_{ts}^* $	0.040

by LHCb [11] as well as the existing lattice QCD predictions [18]. We do not present the results for e in the presentations, since the predictions for the e channel are very close to those of μ .

From Figs. 1–6, we see that

- (1) For all lepton channels, the SMLCSR and RS_c models have roughly the same predictions except for some values of q^2 at which there are small differences between predictions of the SMLCSR and RS_c models on the differential branching ratio.
- (2) The areas swept by the SMLCSR are wider compared to those of lattice QCD [18] existing in the μ channel, but they include those predictions.
- (3) The experimental data in the intervals $4 \text{ GeV}^2/c^4 \leq q^2 \leq 6 \text{ GeV}^2/c^4$ and $18 \text{ GeV}^2/c^4 \leq q^2 \leq 20 \text{ GeV}^2/c^4$ cannot be described by the SMLCSR, lattice QCD, or RS_c models. In the remaining intervals, the SMLCSR, lattice, and RS_c models reproduce

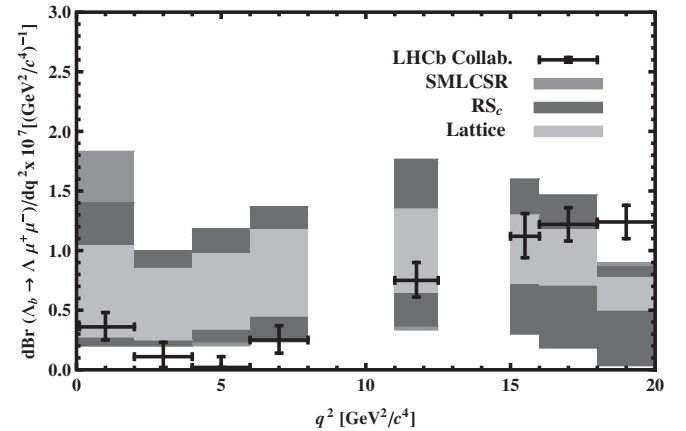


FIG. 1. The dependence of the differential branching ratio on q^2 for the $\Lambda_b \rightarrow \Lambda \mu^+ \mu^-$ transition in the SMLCSR and RS_c models. The lattice QCD [18] and recent experimental data by the LHCb [11] Collaboration are also included.

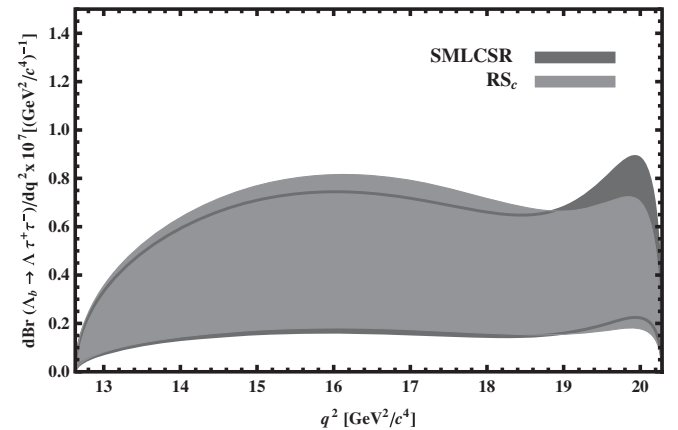


FIG. 2. The dependence of the differential branching ratio on q^2 for the $\Lambda_b \rightarrow \Lambda \tau^+ \tau^-$ transition in the SMLCSR and RS_c models.

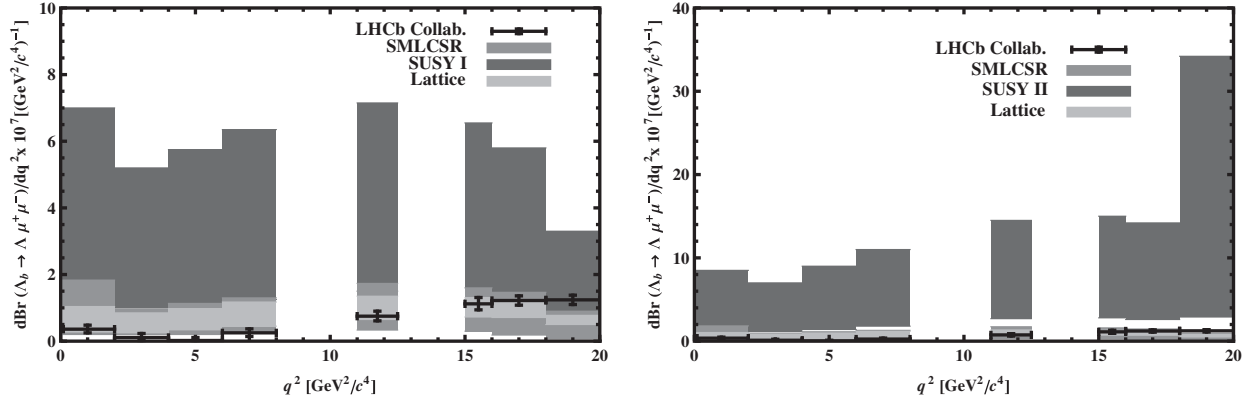


FIG. 3. The dependence of the differential branching ratio on q^2 for the $\Lambda_b \rightarrow \Lambda\mu^+\mu^-$ transition in the SMLCSR and SUSY I and II models. The lattice QCD [18] and recent experimental data by the LHCb [11] Collaboration are also included.

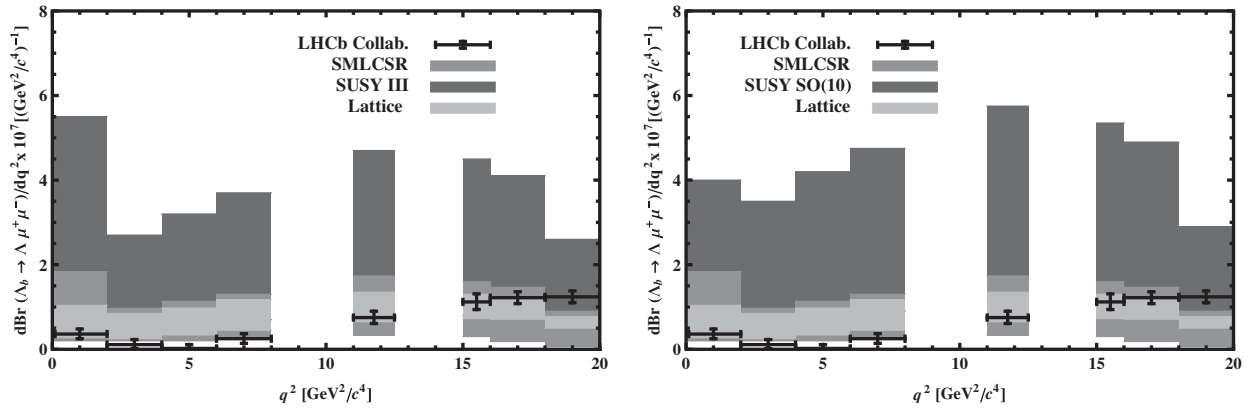


FIG. 4. The dependence of the differential branching ratio on q^2 for the $\Lambda_b \rightarrow \Lambda\mu^+\mu^-$ transition in the SMLCSR and SUSY III and SO(10) models. The lattice QCD [18] and recent experimental data by the LHCb [11] Collaboration are also included.

the experimental data, except for $6 \text{ GeV}^2/c^4 \leq q^2 \leq 8 \text{ GeV}^2/c^4$, for which the datum remains outside of the lattice predictions.

- (4) In the τ channel, the bands of the SMLCSR and RS_c scenarios intersect each other, except for higher values

of q^2 for which the errors of the form factors do not kill the differences between the two model predictions.

- (5) At all lepton channels, the SUSY models show overall considerable deviations from the SMLCSR, lattice QCD, and experimental data, although they

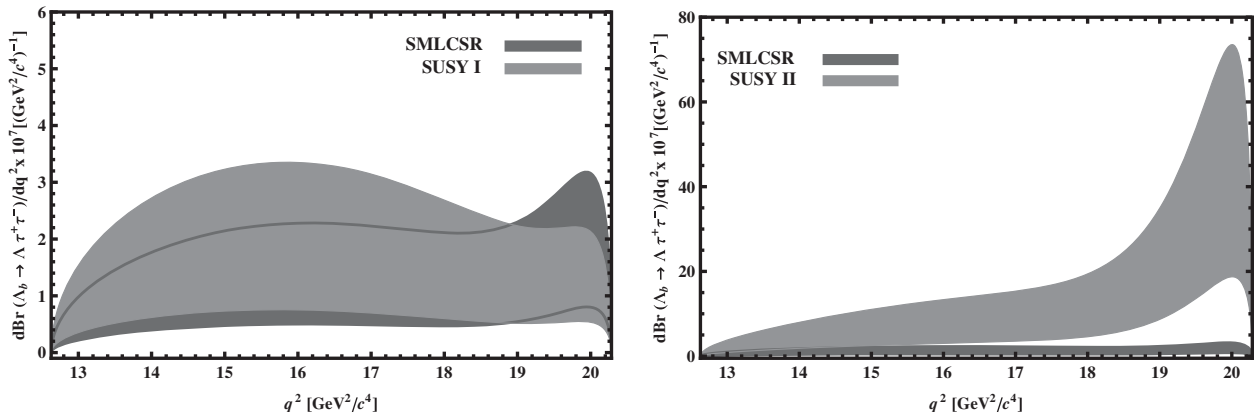


FIG. 5. The dependence of the differential branching ratio on q^2 for the $\Lambda_b \rightarrow \Lambda\tau^+\tau^-$ transition in the SMLCSR and SUSY I and II models.

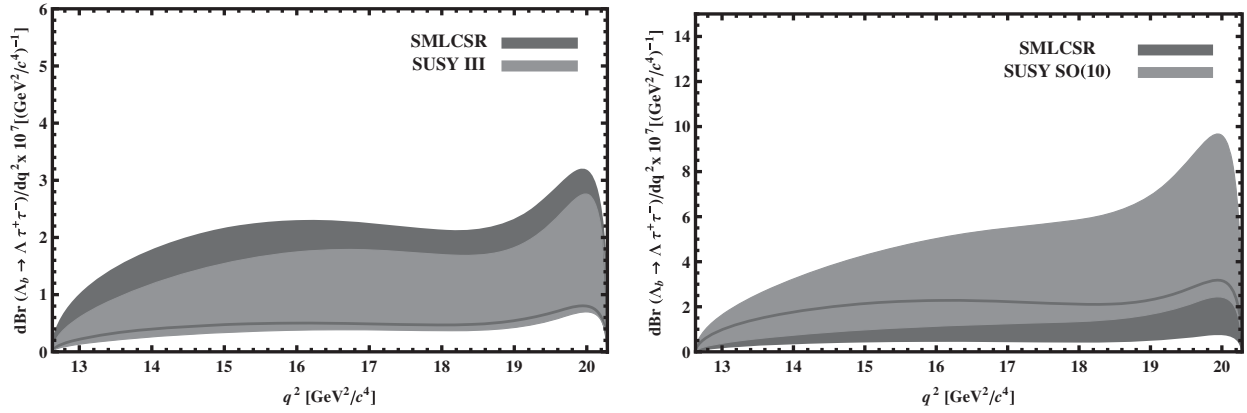


FIG. 6. The dependence of the differential branching ratio on q^2 for the $\Lambda_b \rightarrow \Lambda \tau^+ \tau^-$ transition in the SMLCSR and SUSY III and SO(10) models.

include the predictions of these models for some values of q^2 . The maximum deviations of the SUSY predictions from the results of SMLCSR, lattice QCD, and experiment belongs to the SUSY II model such that the SMLCSR, lattice QCD, and experimental results remain out of the regions swept by the SUSY II model at higher values of q^2 .

- (6) In the μ channel, the experimental data in the interval $18 \text{ GeV}^2/c^4 \leq q^2 \leq 20 \text{ GeV}^2/c^4$ are reproduced by SUSY I, III, and SO(10), but not by SUSY II. Note that in this interval other models (SMLCSR, lattice QCD, and RS_c) also cannot describe the experimental data.
- (7) Again in the μ channel, the experimental data in the interval $4 \text{ GeV}^2/c^4 \leq q^2 \leq 6 \text{ GeV}^2/c^4$ cannot be reproduced by any SUSY models like the SMLCSR, lattice QCD, and RS_c scenarios.
- (8) In the case of τ as the final lepton, there are considerable differences between different SUSY models' predictions and that of the SMLCSR, and these cannot be completely killed by the errors of form factors. The maximum deviations of the SUSY results from the SMLCSR predictions belong to the SUSY II at higher q^2 values.

C. The lepton forward-backward asymmetry

In this subsection, we would like to present the results of the lepton forward-backward asymmetry obtained in different scenarios. The lepton \mathcal{A}_{FB} is defined as

$$\mathcal{A}_{FB}(\hat{s}) = \frac{\int_0^1 \frac{d^2\Gamma}{dsdz}(z, \hat{s}) dz - \int_{-1}^0 \frac{d^2\Gamma}{dsdz}(z, \hat{s}) dz}{\int_0^1 \frac{d^2\Gamma}{dsdz}(z, \hat{s}) dz + \int_{-1}^0 \frac{d^2\Gamma}{dsdz}(z, \hat{s}) dz}. \quad (3.6)$$

Considering the form factors with their uncertainties from Ref. [19], we plot the dependence of the lepton forward-backward asymmetry on q^2 for the decay under consideration in both lepton channels in the SMLCSR,

RS_c , and different SUSY models in Figs. 7–12. From these figures, we obtain that

- (1) In the μ channel, the SMLCSR, lattice QCD, and RS_c models' predictions on \mathcal{A}_{FB} coincide with each

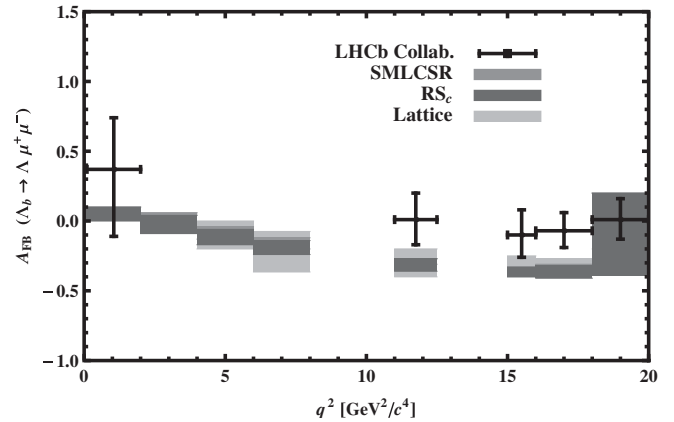


FIG. 7. The dependence of \mathcal{A}_{FB} on q^2 for the $\Lambda_b \rightarrow \Lambda \mu^+ \mu^-$ transition in the SMLCSR, lattice QCD [18], and RS_c models together with recent experimental data by LHCb [11].

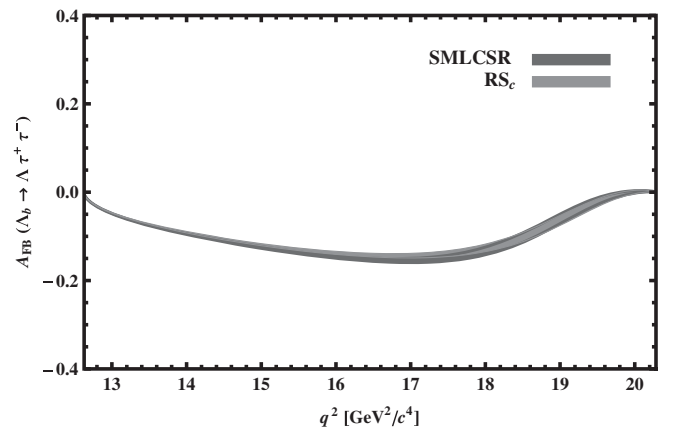


FIG. 8. The dependence of \mathcal{A}_{FB} on q^2 for the $\Lambda_b \rightarrow \Lambda \tau^+ \tau^-$ transition in the SMLCSR and RS_c models.

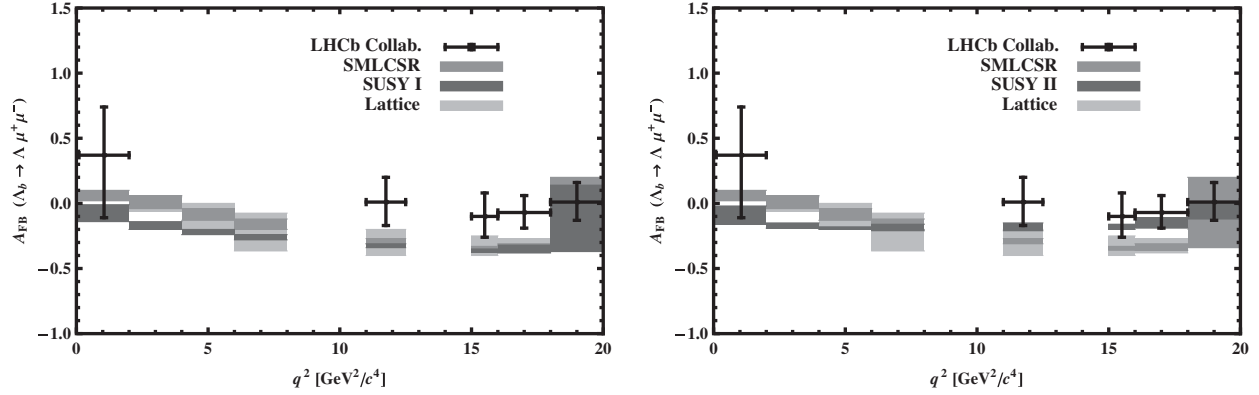


FIG. 9. The dependence of \mathcal{A}_{FB} on q^2 for the $\Lambda_b \rightarrow \Lambda \mu^+ \mu^-$ transition in the SMLCSR, lattice QCD [18], and SUSY I and II models together with recent experimental data by LHCb [11].

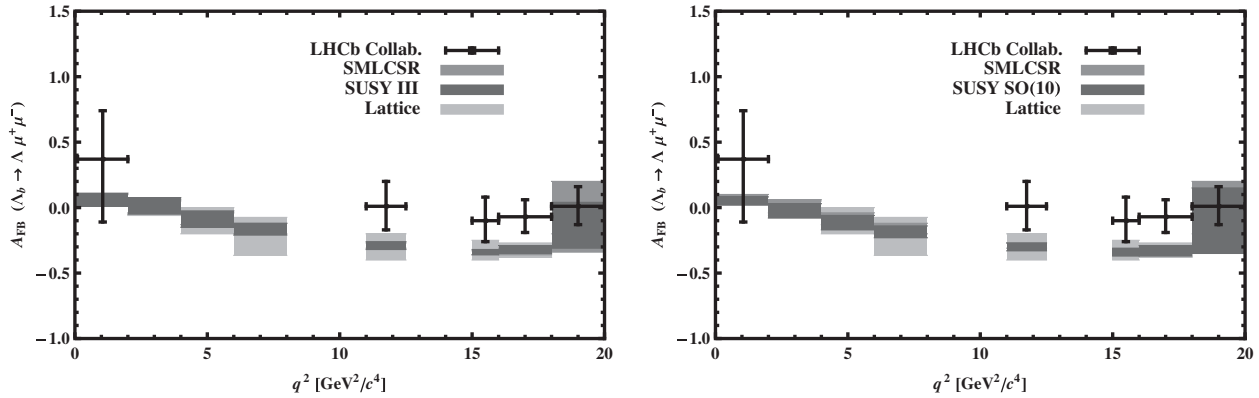


FIG. 10. The dependence of \mathcal{A}_{FB} on q^2 for the $\Lambda_b \rightarrow \Lambda \mu^+ \mu^-$ transition in the SMLCSR, lattice QCD [18], and SUSY III and SO(10) models together with recent experimental data by LHCb [11].

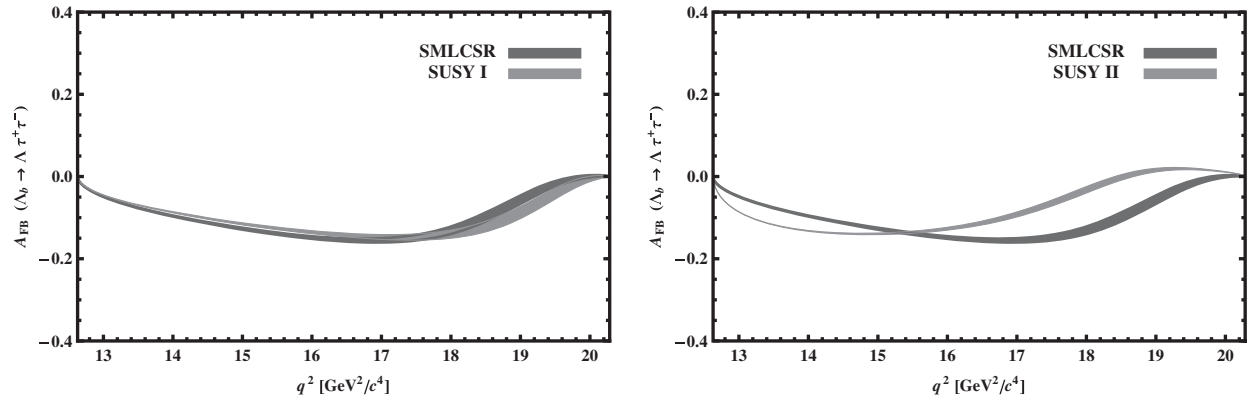


FIG. 11. The dependence of \mathcal{A}_{FB} on q^2 for the $\Lambda_b \rightarrow \Lambda \tau^+ \tau^-$ transition in the SMLCSR and SUSY I and II scenarios.

other. Except for the lattice QCD, they can only describe the experimental data existing in the $0 \text{ GeV}^2/c^4 \leq q^2 \leq 2 \text{ GeV}^2/c^4$ and $18 \text{ GeV}^2/c^4 \leq q^2 \leq 20 \text{ GeV}^2/c^4$ regions. The remaining data lie out of the swept regions by all these models.

- (2) As far as the SUSY models are considered, in the μ channel, the SUSY models have predictions that

deviate from the SMLCSR and lattice QCD predictions considerably. All SUSY models reproduce the experimental data in the regions $0 \text{ GeV}^2/c^4 \leq q^2 \leq 2 \text{ GeV}^2/c^4$ and $18 \text{ GeV}^2/c^4 \leq q^2 \leq 20 \text{ GeV}^2/c^4$. The other data also remain out of the regions swept by different SUSY models, except for SUSY II, which reproduces the experimental

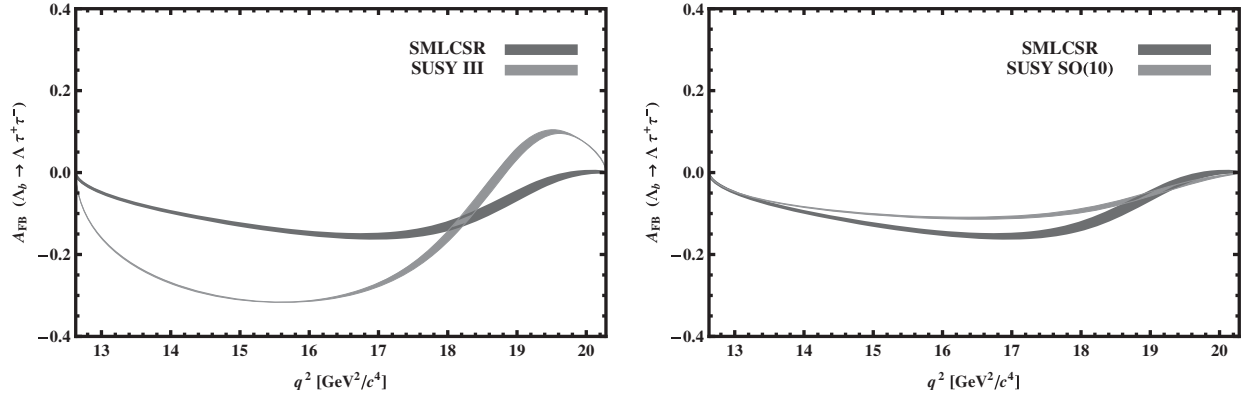


FIG. 12. The dependence of \mathcal{A}_{FB} on q^2 for the $\Lambda_b \rightarrow \Lambda \tau^+ \tau^-$ transition in the SMLCSR and SUSY III and SO(10) scenarios.

data also in the interval $15 \text{ GeV}^2/c^4 \leq q^2 \leq 18 \text{ GeV}^2/c^4$.

- (3) In the case of the τ lepton, the SMLCSR and RS_c have roughly the same predictions on \mathcal{A}_{FB} .
- (4) In the τ lepton channel, the SMLCSR and SUSY I have roughly the same predictions for \mathcal{A}_{FB} ; however, the remaining SUSY models' predictions deviate from the SMLCSR predictions considerably, although they intersect each other at some points.

IV. CONCLUSION

In the present work, we have analyzed the semileptonic $\Lambda_b \rightarrow \Lambda \ell^+ \ell^-$ decay mode in SMLCSR, different SUSY models, and the RS_c scenario. Using the form factors calculated in light-cone QCD sum rules in the full theory [19], we evaluated the differential branching ratio and lepton forward-backward asymmetry for different leptons in those scenarios. We also compared the results obtained via SMLCSR, RS_c , and different SUSY scenarios with the recent experimental data provided by LHCb [11] as well as the existing lattice QCD predictions [18] on the considered quantities. We observed that the regions swept by the SMLCSR model include the RS_c predictions, although they are somewhat wider compared to those of RS_c models for the considered physical quantities. The SMLCSR predictions on the considered quantities in the present work are overall consistent with the lattice QCD predictions provided by Ref. [18].

The predictions of different SUSY models on the differential branching ratio deviate considerably from the SMLCSR and lattice predictions. The maximum deviations

belong to the SUSY II model. In the case of \mathcal{A}_{FB} and the μ channel, the predictions of different SUSY models have considerable deviations from the SMLCSR and lattice QCD predictions. For \mathcal{A}_{FB} and the τ channel, the SUSY I and SMLCSR have roughly the same predictions, but the other SUSY models have predictions different from that of the SMLCSR.

The experimental data on the differential branching ratio in the μ channel can be reproduced by SMLCSR, lattice QCD, and RS_c models, except for the intervals $4 \text{ GeV}^2/c^4 \leq q^2 \leq 6 \text{ GeV}^2/c^4$ and $18 \text{ GeV}^2/c^4 \leq q^2 \leq 20 \text{ GeV}^2/c^4$, which cannot be described by SMLCSR, lattice QCD, or RS_c models. As far as the SUSY models are considered, different SUSY models also cannot reproduce the experimental data in the interval $4 \text{ GeV}^2/c^4 \leq q^2 \leq 6 \text{ GeV}^2/c^4$. However, except for SUSY II, the remaining SUSY scenarios can explain the experimental data in the region $18 \text{ GeV}^2/c^4 \leq q^2 \leq 20 \text{ GeV}^2/c^4$.

In the case of \mathcal{A}_{FB} and the μ channel, the SMLCSR, RS_c , and different SUSY models can only describe the experimental data existing in the $0 \text{ GeV}^2/c^4 \leq q^2 \leq 2 \text{ GeV}^2/c^4$ and $18 \text{ GeV}^2/c^4 \leq q^2 \leq 20 \text{ GeV}^2/c^4$ regions. The other existing data remain out of the swept areas by these models, except for SUSY II, which can also reproduce the experimental data in $15 \text{ GeV}^2/c^4 \leq q^2 \leq 18 \text{ GeV}^2/c^4$.

More experimental data in the μ channel related to different physical quantities associated with the $\Lambda_b \rightarrow \Lambda \mu^+ \mu^-$ mode, future experimental data in the τ channel, and comparison of the results with our predictions on the quantities considered in the present work may help us in the course of searching for new physics effects.

- [1] G. Aad *et al.* (ATLAS Collaboration), Observation of a new particle in the search for the standard model Higgs boson with the ATLAS detector at the LHC, *Phys. Lett. B* **716**, 1 (2012).
- [2] S. Chatrchyan *et al.* (CMS Collaboration), Observation of a new boson at a mass of 125 GeV with the CMS experiment at the LHC, *Phys. Lett. B* **716**, 30 (2012).
- [3] S. Aad *et al.* (ATLAS and CMS Collaborations), Combined Measurement of the Higgs Boson Mass in pp Collisions at $\sqrt{s} = 7$ and 8 TeV with the ATLAS and CMS Experiments, *Phys. Rev. Lett.* **114**, 191803 (2015).
- [4] V. Khachatryan *et al.* (CMS Collaboration), Precise determination of the mass of the Higgs boson and tests of compatibility of its couplings with the standard model predictions using proton collisions at 7 and 8 TeV, *Eur. Phys. J. C* **75**, 212 (2015).
- [5] G. Aad *et al.* (ATLAS Collaboration), Measurement of the Higgs boson mass from the $H \rightarrow \gamma\gamma$ and $H \rightarrow ZZ^* \rightarrow 4\ell$ channels with the ATLAS detector using 25 fb⁻¹ of pp collision data, *Phys. Rev. D* **90**, 052004 (2014).
- [6] V. Khachatryan *et al.* (CMS Collaboration), Observation of the diphoton decay of the Higgs boson and measurement of its properties, *Eur. Phys. J. C* **74**, 3076 (2014).
- [7] S. Chatrchyan *et al.* (CMS Collaboration), Measurement of the properties of a Higgs boson in the four-lepton final state, *Phys. Rev. D* **89**, 092007 (2014).
- [8] A. Pich, ICHEP 2014 summary: Theory status after the first LHC run, [arXiv:1505.01813](https://arxiv.org/abs/1505.01813).
- [9] A. Pich, Status after the first LHC run: Looking for new directions in the physics landscape, [arXiv:1507.01250](https://arxiv.org/abs/1507.01250).
- [10] Ch.-J. Lee and J. Tandean, Minimal lepton flavor violation implications of the $b \rightarrow s$ anomalies, *J. High Energy Phys.* **08** (2015) 123.
- [11] F. Alessio *et al.* (LHCb Collaboration), Differential branching fraction and angular analysis of $\Lambda_b^0 \rightarrow \Lambda\mu^+\mu^-$ decays, *J. High Energy Phys.* **06** (2015) 115.
- [12] T. Gutsche, M. A. Ivanov, J. G. Korner, V. E. Lyubovitskij, and P. Santorelli, Rare baryon decays $\Lambda_b \rightarrow \Lambda\ell^+\ell^-$ ($\ell = e, \mu, \tau$) and $\Lambda_b \rightarrow \Lambda\gamma$: Differential and total rates, lepton- and hadron-side forward-backward asymmetries, *Phys. Rev. D* **87**, 074031 (2013).
- [13] K. Azizi, S. Kartal, A. T. Olgun, and Z. Tavukoglu, Analysis of the semileptonic $\Lambda_b \rightarrow \Lambda\ell^+\ell^-$ transition in topcolor-assisted technicolor (TC2) model, *Phys. Rev. D* **88**, 075007 (2013).
- [14] Y.-L. Wen, C.-X. Yue, and J. Zhang, Rare baryonic decays $\Lambda_b \rightarrow \Lambda\ell^+\ell^-$ in the TTM model, *Int. J. Mod. Phys. A* **28**, 1350075 (2013).
- [15] Y. Liu, L.-L. Liu, and X.-H. Guo, Study of $\Lambda_b \rightarrow \Lambda\ell^+\ell^-$ and $\Lambda_b \rightarrow p\ell\bar{\nu}$ decays in the Bethe-Salpeter equation approach, [arXiv:1503.06907](https://arxiv.org/abs/1503.06907).
- [16] L. Mott and W. Roberts, Lepton polarization asymmetries for FCNC decays of the Λ_b baryon, *Int. J. Mod. Phys. A* **30**, 1550172 (2015).
- [17] T. Feldmann and M. W. Y. Yip, Form factors for $\Lambda_b \rightarrow \Lambda$ transitions in SCET, *Phys. Rev. D* **85**, 014035 (2012).
- [18] W. Detmold, C.-J. David Lin, S. Meinel, and M. Wingate, $\Lambda_b \rightarrow \Lambda\ell^+\ell^-$ form factors and differential branching fraction from lattice QCD, *Phys. Rev. D* **87**, 074502 (2013).
- [19] T. M. Aliev, K. Azizi, and M. Savci, Analysis of the $\Lambda_b \rightarrow \Lambda\ell^+\ell^-$ decay in QCD, *Phys. Rev. D* **81**, 056006 (2010).
- [20] C.-H. Chen and C. Q. Ceng, Lepton asymmetries in heavy baryon decays of $\Lambda_b \rightarrow \Lambda\ell^+\ell^-$, *Phys. Lett. B* **516**, 327 (2001).
- [21] M. Misiak, The $b \rightarrow se^+e^-$ and $b \rightarrow s\gamma$ decays with next-to-leading logarithmic QCD-corrections, *Nucl. Phys.* **B393**, 23 (1993); *Nucl. Phys.* **B439**, 461 (1995).
- [22] A. J. Buras and M. Muenz, Effective Hamiltonian for $B \rightarrow X_s e^+e^-$ beyond leading logarithms in the NDR and HV schemes, *Phys. Rev. D* **52**, 186 (1995).
- [23] A. J. Buras, Weak Hamiltonian, CP violation and rare decays, [arXiv:hep-ph/9806471](https://arxiv.org/abs/hep-ph/9806471).
- [24] A. J. Buras, M. Misiak, M. Muenz, and S. Pokorski, Theoretical uncertainties and phenomenological aspects of $B \rightarrow X_s\gamma$ decay, *Nucl. Phys.* **B424**, 374 (1994).
- [25] M. J. Aslam, Y.-M. Wang, and C.-D. Lü, Exclusive semileptonic decays of $\Lambda_b \rightarrow \Lambda l^+ l^-$ in supersymmetric theories, *Phys. Rev. D* **78**, 114032 (2008).
- [26] A. Ahmed, I. Ahmed, M. A. Paracha, M. Junaid, A. Rehman, and M. J. Aslam, Comparative study of $B_c \rightarrow D_s^* \ell^+ \ell^-$ decays in standard model and supersymmetric models, [arXiv:1108.1058](https://arxiv.org/abs/1108.1058).
- [27] Q.-Sh. Yan, Ch.-Sh. Huang, L. Wei, and Sh.-H. Zhu, Exclusive semileptonic rare decays $B \rightarrow (K, K^*) \ell^+ \ell^-$ in supersymmetric theories, *Phys. Rev. D* **62**, 094023 (2000).
- [28] W.-J. Li, Y.-B. Dai, and Ch.-Sh. Huang, Exclusive semileptonic rare decays $B \rightarrow K^{(*)} l^+ l^-$ in a SUSY SO(10) GUT, *Eur. Phys. J. C* **40**, 565 (2005).
- [29] M. J. Aslam, C.-D. Lu, and Y.-M. Wang, $B \rightarrow K_0^*(1430) l^+ l^-$ decays in supersymmetric theories, *Phys. Rev. D* **79**, 074007 (2009).
- [30] L. Randall and R. Sundrum, A Large Mass Hierarchy from a Small Extra Dimension, *Phys. Rev. Lett.* **83**, 3370 (1999).
- [31] L. Randall and R. Sundrum, An Alternative to Compactification, *Phys. Rev. Lett.* **83**, 4690 (1999).
- [32] S. Casagrande, F. Goertz, U. Haisch, M. Neubert, and T. Pfoh, The custodial Randall-Sundrum model: From precision tests to Higgs physics, *J. High Energy Phys.* **09** (2010) 014.
- [33] M. Blanke, K and B physics in the custodially protected Randall-Sundrum model, *Proc. Sci.*, EPS-HEP2009 (2009) 196.
- [34] P. Biancofiore, P. Colangelo, and F. De Fazio, Rare semileptonic $B \rightarrow K^* \ell^+ \ell^-$ decays in RS_c model, *Phys. Rev. D* **89**, 095018 (2014).
- [35] M. Blanke, A. J. Buras, B. Duling, S. Gori, and A. Weiler, $\Delta F = 2$ observables and fine-tuning in a warped extra dimension with custodial protection, *J. High Energy Phys.* **03** (2009) 001.
- [36] M. Blanke, A. J. Buras, B. Duling, K. Gemmler, and S. Gori, Rare K and B decays in a warped extra dimension with custodial protection, *J. High Energy Phys.* **03** (2009) 108.
- [37] B. Duling, K and B meson mixing in warped extra dimensions with custodial protection, *J. Phys. Conf. Ser.* **171**, 012061 (2009).
- [38] M. E. Albrecht, M. Blanke, A. J. Buras, B. Duling, and K. Gemmler, Electroweak and flavour structure of a warped

- extra dimension with custodial protection, *J. High Energy Phys.* **09** (2009) 064.
- [39] M. Blanke, B. Shakya, P. Tanedo, and Y. Tsai, The birds and the B_s in RS: The $b \rightarrow s\gamma$ penguin in a warped extra dimension, *J. High Energy Phys.* **08** (2012) 038.
- [40] P. Biancofiore, P. Colangelo, F. De Fazio, and E. Scrimieri, Exclusive $b \rightarrow s\nu\bar{\nu}$ induced transitions in RS_c model, *Eur. Phys. J. C* **75**, 134 (2015).
- [41] K. A. Olive *et al.* (Particle Data Group), Review of Particle Physics, *Chin. Phys. C* **38**, 090001 (2014).